9. Samuelson, R. E., Nath, N. R. & Borysow, A. Gaseous abundances and methane supersaturation in Titan's tropopause. *Planet. Space Sci.* **45,** 959–980 (1997).
10. Griffith, C. A., Owen, T. & Wagener, R. Titan's surface and trophosphere, investigated with ground-based, near-infrared observations. *Icarus* **93,** 362–378 (1991).
11. Lemmon, M. T., Karkoschka, E. & Tomasko, M. Titan's rotation: surface feature observed. *Icarus* **103,** 329–332 (1993).
12. Griffith, C. A. Evidence for surface heterogeneity on Titan. *Nature* **364,** 511–513 (1993).
13. Noll, K. S., Geballe, T. S., Knacke, R. F. & Pendleton, Y. J. Titan's 5 μm spectral window: carbon monoxide and the albedo of the surface. *Icarus* **124,** 625–631 (1996).
14. Muhleman, D. O., Grossman, A. W., Butler, B. J. & Slade, M. A. Radar reflectivity of Titan. *Science* **248,** 975–980 (1990).
15. Smith, P. H. *et al.* Titan's surface revealed by HST imaging. *Icarus* **119,** 336–349 (1996).
16. Combes, M. *et al.* Spatially resolved images of Titan by means of adaptive optics. *Icarus* **129,** 482–497 (1997).
17. Lemmon, M. T., Karkoschka, E. & Tomasko, M. Titan's rotational light-curve. *Icarus* **113,** 27–38 (1995).
18. Coustenis, A., Lellouch, E., Maillard, J. P. & McKay, C. P. Titan's surface: composition and variability from its near-infrared albedo. *Icarus* **118,** 87–104 (1995).
19. Khare, B. N. *et al.* Optical constants of organic tholins produced in a simulated Titanian atmosphere: from soft X-ray to microwave frequencies. *Icarus* **60,** 127–137 (1984).
20. Husson, N., Bonnet, B., Scott, N. A. & Chédin, A. *The "GEISA" data bank, 1991 version* (Int. note L.M.D. 163, Lab. de Météorologie Dynamique, Palaiseau, 1991).
21. Rages, K., Pollack, J. B. & Smith, P. H. Size estimates of Titan's aerosols based on Voyager high-phase-angle images. *J. Geophys. Res.* **88,** 8721–8728 (1983).
22. McKay, C. P., Pollack, J. B. & Courtin, R. The thermal structure of Titan's atmosphere. *Icarus* **80,** 23–53 (1989).
23. Toon, O. B., McKay, C. P., Griffith, C. A. & Turco, R. P. A physical model of Titan's aerosols. *Icarus* **95,** 24–53 (1992).
24. Strong, K., Taylor, F. W., Calcutt, S. B., Remedios, J. J. & Ballard, J. Spectral parameters of self- and hydrogen-broadened methane from 2000 to 9500 cm^{-1} for remote sounding of the atmosphere of Jupiter. *J. Quant. Spectrosc. Rad. Transfer* **50,** 363–429 (1993).
25. Calvin, W. M. & Clark, R. N. Modeling the reflectance spectrum of Callisto 0.25 to 4.1 μm. *Icarus* **89,** 305–317 (1991).

Acknowledgements. We thank C. McKay for conversations on the weather, M. Flasar for suggestions that improved the paper, K. Noll for a helpful reading and C. B. Phillips for help in operating arduous radiative transfer codes. C.G. was supported by an NSF Young Investigator Award, the Research Corporation, and the NASA Planetary Astronomy Program.

Correspondence and requests for materials should be addressed to C.A.G. (e-mail: griffith@vela.phy.nau.edu).

Mesoscopic behaviour of the neutral Fermi gas ^{3}He confined in quantum wires

S. L. Phillipson*, A. M. Guénault*, S. N. Fisher*, G. R. Pickett* & P. J. Y. Thibault*†

* *Department of Physics, Lancaster University, Lancaster LA1 4YB, UK*

The behaviour of electron gases in restricted geometries provides a means to explore the fundamental quantum-mechanical properties of fermion gases at mesoscopic length scales[1]. But the existence of Coulomb repulsion between electrons unavoidably complicates the physics. Quantum gases of neutral fermions—such as ^{3}He quasiparticles in a dilute solution of ^{3}He in ^{4}He, cooled to millikelvin temperatures[2]—therefore offer a means of probing regimes completely inaccessible to electronic systems. Here we demonstrate the quantum exclusion of a ^{3}He fermion gas from a network of narrow channels, connected to a reservoir of ^{3}He/^{4}He solution. The effect is expected from simple quantum-mechanical arguments, which predict that the ^{3}He atoms cannot enter the channels when their wavelength exceeds √2 times the channel width. By adjusting the temperature of the solution, the energy of the particles and hence their average wavelength can be controlled. In this way, we observe temperature-dependent changes in the penetration of the ^{3}He quasiparticles into the channels. Our results demonstrate the macroscopic response of an atomic gas to basic quantum-mechanical restrictions at the mesoscopic level.

Although the ^{3}He gas in dilute ^{3}He/^{4}He solutions might be expected to show broadly similar behaviour to that of an electron gas when similarly confined, this Fermi–Dirac quantum fluid has a number of advantages over the usual metallic or semiconducting systems. The medium can be readily decanted into a container shaped to provide the requisite restricted geometry and therefore various solutions can be studied under identical conditions. The ^{3}He solutions are absolutely clean at millikelvin temperatures and thus there are no impurity effects. The Fermi parameters of the ^{3}He—Fermi energy E_F, Fermi temperature T_F and Fermi wavelength λ_F—can be varied over a wide range by adjustment of the ^{3}He concentration. Finally, unlike in the charged electron gas, the potential energy determining the bottom of the excitation band is only a very weak function of the local particle density and there are no problems of Coulomb repulsion.

The Fermi temperature of a dilute ^{3}He/^{4}He solution of fractional ^{3}He concentration x varies as $x^{2/3}$. A 0.1% ^{3}He solution yields a Fermi energy of around 26 mK with an associated Fermi wavelength of 8 nm. This is much smaller than would be practicable in electronic systems, but with helium solutions we can make use of confined geometries on this scale over the temperature range 5–100 mK which is readily accessible with a dilution refrigerator.

The experiment reported here, the detection of the quantum exclusion of the ^{3}He gas from a system of narrow channels as the temperature is reduced, was chosen for two reasons. First, it is conceptually simple, and second, it has no direct analogue in an electronic system, as quantum exclusion of an electron gas leads to a change in the local potential which largely cancels the effect. Furthermore, a metallic system cannot be probed over a temperature range spanning T_F.

The principle of an ideal experiment is illustrated in Fig. 1. A bulk ^{3}He/^{4}He solution is placed in contact with a network of narrow cavities with a scale dimension of a. The ^{3}He concentration is adjusted such that the Fermi wavelength is longer than $\sqrt{2}a$, or in other words, the confinement energy (E_0, of the order of $h^2/4m^*a^2$, where m^* is the ^{3}He effective mass) is greater than kT_F. Therefore, at temperatures well below T_F, ^{3}He atoms cannot penetrate into the cavities. However, as the temperature is increased, at some point the most energetic atoms begin to penetrate. This starts to occur significantly when $(E_F + 2kT)$ exceeds the confinement energy E_0. Therefore, if over the temperature range used the quantity $(E_F + 2kT)$ can be made to span the confinement energy, then at the low-temperature end ^{3}He is totally excluded from the pores but will be able to penetrate into them at the higher temperatures. We should therefore see an increase in the concentration of ^{3}He in the pores with increasing temperature.

The confined geometry is provided by the channels in porous Vycor glass which have[3] a characteristic dimension a of around 7 nm. Given the accepted value[2] for the effective mass m^* for ^{3}He quasiparticles as 2.25 times the bare ^{3}He atomic mass, the expected confinement energy E_0 is 15 mK in temperature units. This is a little low to implement the ideal experiment, as the lowest reliable temperature to which we can cool the cell is around 8 mK, meaning that kT is rather large even at our base temperature. However, calculations show that even with a 0.1% ^{3}He solution there should be a significant change of the pore penetration with temperature, and this concentration was chosen. For more dilute solutions much of the variation would occur below 8 mK, and also the measurable effect would be smaller.

We infer the extent of the penetration of ^{3}He into the pores from the concentration of ^{3}He in the external bulk solution; the bulk concentration is monitored by a capacitative measurement of the dielectric constant of the solution. As the changes in dielectric constant with changes in ^{3}He concentration are small, we must ensure that the volume of bulk solution in our experimental cell is as small as possible in comparison with the pore volume. The bulk volume must accommodate both the capacitor for measuring the ^{3}He concentration and pads of silver sinter necessary to make thermal contact to the solution. (The sinter pore size is ~100 nm

† Present address: Centre de Recherche sur les Très Basses Températures, CNRS, BP166, 38042 Grenoble cedex 9, France.

and hence qualifies as "bulk" volume.) The pore volume in the Vycor represents 17% of the total helium volume of the cell. This figure is determined from the quantity of helium required to fill the cell along with the known volume of the Vycor glass, and the knowledge[3] that the pores in the Vycor represent 30% of the bulk Vycor volume. The cell is thermally anchored to the mixing chamber of a 2 mK dilution refrigerator[4].

The principle of the measurement is straightforward. The dilute solution fills the adjacent bulk and confined regions. At low temperatures, the energy of a significant fraction of the ^{3}He atoms in the solution is lower than the pore confinement energy, and these atoms are excluded from the Vycor. The ^{4}He component being superfluid can penetrate freely. As the temperature is increased, the Fermi distribution becomes wider, the fraction of ^{3}He atoms excluded falls, and thus the degree of penetration into the pores increases. This leads to a fall in the ^{3}He concentration in the bulk region which we can monitor. Since the ^{3}He atomic volume is larger than that of ^{4}He, with falling ^{3}He concentration the number of helium atoms in the capacitor rises, hence increasing the capacitance. Thus we should observe the capacitance to increase with increasing temperature.

To perform the experiment, we monitor the capacitance as a function of temperature to infer the changes in ^{3}He density in the Vycor. This procedure requires much care to avoid temperature gradients which can drive ^{3}He around the cell. We take 8 mK as the baseline, measure the capacitance and then monitor the change in capacitance as the temperature is increased. The temperature of the cell is adjusted by stabilizing the temperature of the mixing chamber of the dilution refrigerator, achieved by heating the final heat exchanger. Thermal equilibrium in the cell is typically reached only some 3 hours after the temperature is changed; thereafter, the cell must be left for at least a further 3 hours to establish the appropriate capacitance value. The heating is then stopped and after a further similar period the 8 mK background value checked. The practical range is limited by the lowest temperature at which we can reliably maintain the cell in thermal equilibrium with the mixing chamber, 8 mK, and the upper limit of 50 mK above which measurements become difficult owing to increasing temperature instabilities.

As the capacitance changes are so small, we first have to establish the background variation of the capacitance with temperature. We can either measure the capacitance of the ^{3}He/^{4}He solution as a function of temperature with no Vycor in the cell (that is, when there is no effect on the ^{3}He concentration from any quantum confinement), or we can measure the capacitance changes for pure ^{4}He with the Vycor present. Both methods yield the same result,

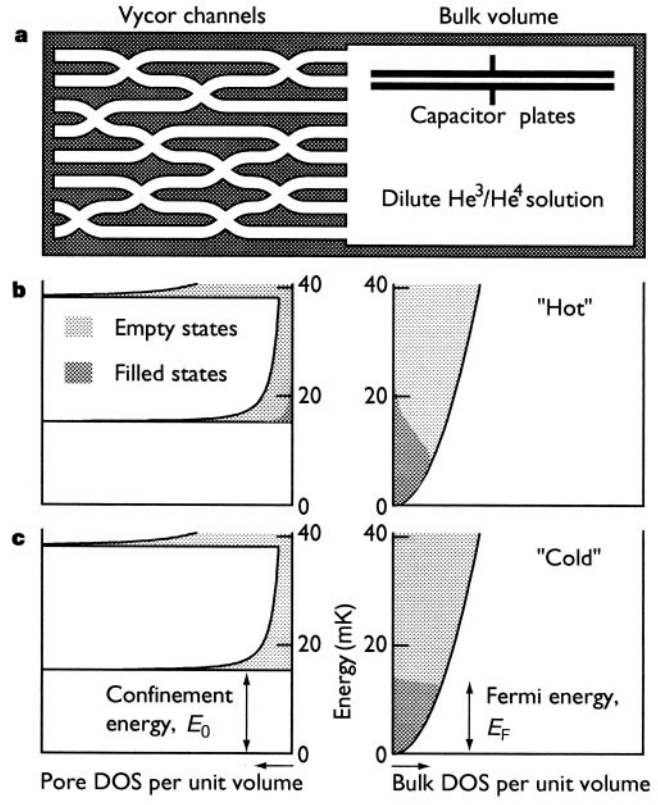

Figure 1 Schematic view of the experiment. In **a**, a dilute ^{3}He/^{4}He solution is contained in a bulk volume in contact with a set of interconnecting 'quantum wires', which in the present case comprise the pores in Vycor glass. Ideally the Fermi energy of the solution should be adjusted to be below the confinement energy of the pores. **b** and **c**, schematic views of the densities of states (DOS) and the disposition of the ^{3}He component in the solution between the two regions as a function of temperature. In **b** the temperature is 'high', and ^{3}He atoms can penetrate into the confined wires, whereas in **c**, where the temperature $T \ll T_F$, ^{3}He is excluded from the restricted volume as there are no occupied states above the confinement energy E_0. The DOS in the quantum wire region is calculated on the basis of the uniform tube model discussed in the text. As the pores are randomly connected, the DOS for the pores would be qualitatively similar but without the large discontinuities shown here. The 'bulk' volume contains a capacitor to measure the ^{3}He concentration. This is a formidable task because the difference in dielectric constant between ^{3}He and ^{4}He is rather small. (The dielectric constant of the solution[6,7] is $\epsilon = 1.0572 - 0.0166x$ where x is the fractional ^{3}He concentration.) The expected change in capacitance is of the order of 1 part in 10^6, which required us to develop a capacitor with at least 1 part in 10^7 stability for satisfactory measurements. The ~10 pF capacitance is measured with an Andeen–Hagerling model 2500 1 kHz automatic capacitance bridge. We monitor the temperature of the cell with a vibrating wire resonator (as described in ref. 4) in the mixing chamber of the dilution refrigerator.

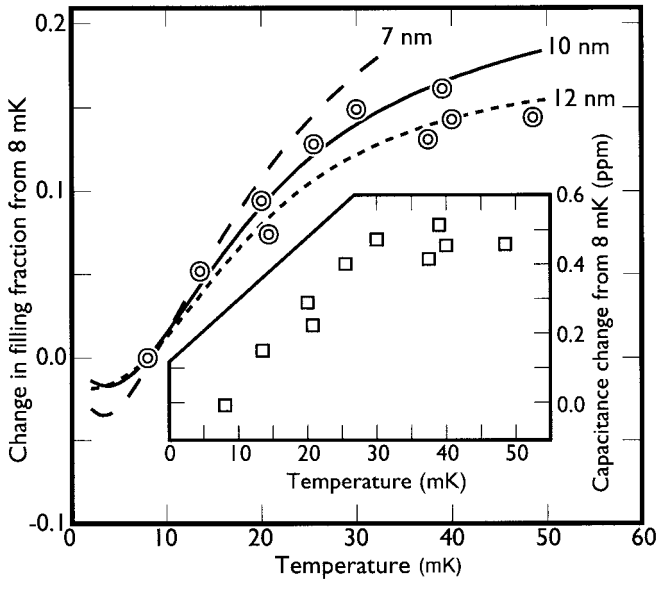

Figure 2 The measured penetration of the ^{3}He. Inset, the change in relative capacitance with temperature of 0.1% ^{3}He/^{4}He solution as a result of the quantum penetration of ^{3}He atoms into the Vycor with increasing temperature. Main figure, the same data converted to the change in relative filling factor in the pores. The curves represent the change in filling factor calculated from a simple uniform 'quantum wire' model as described in the text for pore channel widths of 7, 10 and 12 nm. The absolute filling factor changes from about 0.4 to 0.6 for the 10 nm channels over this temperature range. (The upturn in the calculations below 5 mK arises from the incomplete exclusion at $T = 0$ together with a DOS which falls with increasing energy, see Fig. 1).

namely a fall of about 1.0 p.p.m. in capacitance over the temperature range used. The agreement between the two sets of data, taken in separate runs a few months apart, shows that the capacitor behaves reproducibly at a level of one in 10^7 over a long time period.

Knowing the background capacitance, we can investigate the effect of the quantum exclusion. The measured change in capacitance for a 0.1% ^{3}He in ^{4}He solution with the background subtracted is shown in Fig. 2 inset. The main graph in Fig. 2 shows the data converted to ^{3}He filling factor in the pores, defined as the ratio of ^{3}He concentration in the pores to total ^{3}He concentration in the solution—that is, complete penetration of ^{3}He into the pores corresponds to a filling factor of unity. The conversion requires no adjustable parameters as we know all the volumes in the cell. Figure 2 shows that the filling factor in the pores has increased by 0.2 over our temperature range. The effect of the quantum exclusion with the gradual expulsion of ^{3}He from the confined region as the temperature falls is quite clear. Had we been able to work at a lower temperature and with a concentration approaching the ideal situation of Fig. 1, we should have been able to span a temperature range where the filling factor changed from near zero to unity—that is, from complete exclusion to complete penetration.

We can compare the observed ^{3}He penetration with a calculation made on the basis of a simple single-particle model. Although Vycor glass has a complicated structure, for a zeroth-order model we assume the pores to constitute an array of uniform quantum wires with a square cross-section of width a and with the known total volume. The ^{3}He density of states is then given by the combination of transverse standing-wave states in the square cross-section and the free longitudinal motion. This gives a density of states as a function of energy ϵ made up of a number of $(\epsilon - \epsilon_0)^{-1/2}$ terms in which $\epsilon_0 = (n^2 + l^2)E_0/2$ with $E_0 = h^2/4m^*a^2$, and where n and l are the positive integer quantum numbers defining the transverse state. (The two lowest such terms are those shown in Fig. 1.)

This calculation has just one adjustable parameter, the confinement energy E_0, or equivalently the channel width a. We note that a here is the width open to ^{3}He quasiparticles; this is the bare Vycor channel width minus ~1 nm to allow for the two atomic layers of solid ^{4}He adsorbed on the wall. The density of states so derived may be directly compared with the experiment because there are no other unknowns. We assume that the states are filled with the Fermi Dirac distribution, and compute the chemical potential needed to ensure that the correct total number of ^{3}He quasiparticles occupies the cell. The three curves in Fig. 2 show the filling factor calculated in this way on the assumption that $a = 7$, 10, 12 nm, that is, that $E_0 = 5$, 7.5, 15 mK. Given the simplicity of the assumptions, the agreement between the observed filling factor and the quantum exclusion calculation for $a \approx 10$ nm is good over the whole temperature range.

This agreement confirms that there is indeed a change in the quantum confinement of ^{3}He quasiparticles in narrow channels as a function of temperature. This is, to our knowledge, the first confinement experiment to be performed in helium; with more refined techniques we expect to gain access to a whole range of mesoscopic behaviour which has no analogue in electronic systems. For example, the equivalent of the metal/insulator transition near the critical point is complicated in the charged system by the Coulombic repulsion between the electrons. It would also be interesting to study more dilute solutions and/or narrower channels where E_F could be adjusted to be much smaller than the confinement energy, as with low enough temperatures we would see the complete transition from exclusion to penetration. Finally, we could add an energy $\sim \pm 10$ mK to the confinement energy by applying a high magnetic field, making the quantum exclusion from the channels dependent on the quasiparticle spin. This would greatly enhance the effect for the antiparallel spin, and suggests that a porous membrane in a high magnetic field might provide a ^{3}He polarization filter[5]. □

Received 28 May; accepted 27 July 1998.

1. Sohn, L. L., Kouwenhoven, L. P. & Schön, G. (eds) *Mesoscopic Electron Transport* (NATO ASI Ser, Vol. 345, Kluwer Academic, 1997).
2. Owers-Bradley, J. R. Spin-polarized ^{3}He-^{4}He liquids. *Rep. Prog. Phys.* **60,** 1173–1216 (1998).
3. Levitz, P., Ehret, G., Sinha, S. K. & Drake, J. M. Porous vycor glass—the microstructure as probed by electron microscopy, direct energy transfer, small angle scattering, and molecular adsorption. *J. Chem. Phys.* **95,** 6151–6161 (1991).
4. Bunkov, Yu. M. *et al.* A compact dilution refrigerator with vertical heat exchangers for operation to 2 mK. *J. Low Temp. Phys.* **83,** 257–272 (1991).
5. Ohi, A. & Nakayama, T. Percolative diffusion of dissolved ^{3}He atoms in He II through porous media. *J. Low Temp. Phys.* **81,** 349–368 (1990).
6. Kierstead, H. A. Dielectric constant, molar volume, and phase diagram of saturated ^{3}He-^{4}He mixtures. *J. Low Temp. Phys.* **24,** 497–512 (1976).
7. Castelijns, C. A. M., Kuerten, J. G. M., de Waele, A. T. A. M. & Gijsman, H. M. ^{3}He flow in dilute ^{3}He-^{4}He mixtures at temperatures between 10 and 150 mK. *Phys. Rev. B* **52,** 2870–2886 (1985).

Acknowledgements. We thank V. Fal'ko and A. Volkov for discussions.

Correspondence and requests for materials should be addressed to A.M.G. (e-mail: a.guenault@lancaster.ac.uk).

Spin fluctuations in $YBa_2Cu_3O_{6.6}$

H. A. Mook*, Pengcheng Dai*, S. M. Hayden†, G. Aeppli‡, T. G. Perring§ & F. Doğan‖

** Oak Ridge National Laboratory, Oak Ridge, Tennessee 37831-6393, USA*
† H. H. Wills Physics Laboratory, University of Bristol, Bristol BS8 1TL, UK
‡ NEC Research Institute, 4 Independence Way, Princeton, New Jersey 08540, USA
§ ISIS Facility, Rutherford Appleton Laboratory, Chilton, Didcot OX11 0QX, UK
‖ Department of Materials Sciences and Engineering, University of Washington, Seattle, Washington 98195, USA

An important feature of the high-transition-temperature (high-T_c) copper oxide superconductors is the magnetism that results from the spins associated with the incomplete outer electronic shells ($3d^9$) of the copper ions. Fluctuations of these spins give rise to magnetic excitations of the material, and might mediate the electron pairing that leads to superconductivity. If the mechanism for high-T_c superconductivity is the same for all copper oxide systems, their spin fluctuations should be universal. But so far, the opposite has seemed to be the case: neutron scattering data reveal clear differences between the spin fluctuations for two major classes of high-T_c materials, $La_{2-x}Sr_xCuO_4$ (refs 1–3) and $YBa_2Cu_3O_{7-x}$ (refs 4–6), whose respective building blocks are CuO_2 layers and bilayers. Here we report two-dimensional neutron-scattering imaging of $YBa_2Cu_3O_{6.6}$, which reveals that the low-frequency magnetic excitations are virtually identical to those of similarly doped $La_{2-x}Sr_xCuO_4$. Thus, the high-temperature ($T_c \lesssim 92$ K) superconductivity of the former materials may be related to spatially coherent low-frequency spin excitations that were previously thought to be unique to the lower-T_c (<40 K) single-layer $La_{2-x}Sr_xCuO_4$ family.

The most celebrated common feature of copper oxide magnetism is that the undoped parent compounds are insulating antiferromagnets, characterized by a simple doubling of the crystallographic unit cells in the CuO_2 planes. Neutron scattering, which measures the Fourier transform (in space and time) of the spin–spin correlation function, long ago imaged the doubling[7,8] that manifests itself in diffraction peaks at the wavevectors (1/2, 1/2). To label wavevectors in two-dimensional reciprocal space (Fig. 1a), we use reciprocal lattice units such that (1,0) and (0,1) are along the nearest-neighbour copper–oxygen–copper paths and are the locations of the lowest-order diffraction peaks from the nuclei in the nearly square CuO_2 planes. Upon chemical doping to induce metallic and superconducting behaviours, the elastic diffraction peaks, due to static magnetic order, disappear. Both antiferromagnetic and superconducting compositions show strong inelastic scattering derived from magnetic fluctuations. For superconducting